



Impacts of Activation Energy and Modified Darcy Law on the Motion of Williamson Nanofluid Over a Stretching Riga Sheet Through a Porous Medium

N. T. M. Eldabe¹, A. M. Saeed^{2,*}, A.M. Ismael³, S. M. Ali⁴

¹ *Department of Mathematics, Faculty of Education, Ain Shams University, Roxy, Cairo, Egypt*

² *Department of Mathematics, College of Science, Qassim University, Buraydah 51452, Saudi Arabia*

³ *Department of Mathematics, Faculty of Science, Ain shams University, Abbasiya, Egypt*

⁴ *Department of Basic Engineering Sciences, College of Engineering, Imam Abdulrahman Bin Faisal University, P.O. Box 1982, Dammam, 34151 Saudi Arabia*

Abstract. The present analysis is motivated by the need to elucidate with more accuracy and sophistication the motion of Williamson nanofluid with activation energy and modified darcy law through porous medium over a stretching riga sheet. The problem is modulated mathematically by using the momentum, energy and concentration equations. The nonlinear partial differential equations describe the motion is transformed to nonlinear ordinary differential equations by using a suitable transformations. The obtained system of equations with boundary conditions inside the boundary layer are solved semi analytically by using homotopy perturbation method. The velocity, temperature and the concentration of the fluid as well skin-friction, Nusselt and Sherwood numbers are obtained as a functions of the physical parameters of the problem. The effects of these parameters on the solutions are discussed numerically and illustrated graphically through some figures. It is found that the parameters play a dramatic role to control the solutions. For example the velocity increases with increasing Williamson parameter, permeability parameter and modified Hermann number. On the other hand the fluid temperature increases with increasing both of Brownian parameter and Eckert number. In addition, increasing the activation energy and thermophoresis parameter increases the fluid concentration.

2020 Mathematics Subject Classifications: 76S05, 76D10, 80A32, 35Q79

Key Words and Phrases: Activation energy, riga sheet, nanofluid, magnetohydrodynamic flow

*Corresponding author.

DOI: <https://doi.org/10.29020/nybg.ejpam.v18i1.5616>

Email addresses: eng_mohamed_nabil125@hotmail.com ((N. T. M. Eldabe),
abdulkafi.ahmed@qu.edu.sa (A. M. Saeed), ayaismael1990@gmail.com (A. M. Ismael),
smsali@iau.edu.sa (S. M. Ali)

1. Introduction

The boundary layer refers to the layer of fluid in the immediate vicinity of a boundary surface where the effects of viscosity are significant. A range of velocities occurs across the boundary layer from maximum to zero, provided that the fluid is contact with surface. Generally, boundary layer flows affected by magnetohydrodynamic (MHD) play a critical role in manufacturing and technical processes, including the construction of MHD turbines, flow meters, and nuclear reactors. External magnetic fields are widely used to control high conductivity fluid flows, such as semiconductor melting or liquid metals, referred to as conventional MHD flow. This method is ineffective for fluids with low electrical conductivity, such as sea water. A Riga surface generates Lorentz force. Riga refers to a plate surface containing mutually placed magnets and electrodes. The plate is unique because it induces electromagnetic energy sufficient to generate Lorentz forces along the surface, thereby restricting the flow of slightly conducting fluid. The plate was originally constructed from an array of interspaced and obligatory magnets distributed in a span wise configuration. It can be utilized to prevent boundary layer tearing caused by radiation. In this regard, the Riga plate induced laminar flow has been examined in physical properties. Naseer et al. [18] studied heat transfer and the steady boundary layer flow of a hyperbolic tangent fluid flowing over a vertical potentially stretching cylinder in its axial direction. viscous dissipation and Joule heating influences on the boundary layer flow over a stretching vertical Riga plate of a micropolar nanofluid are discussed by Eldabe et al. [10]. Bilal et al. [5] investigated the thermal characteristics generated in a viscosity-dependent viscoelastic non-linear fluid as it flows over an isothermally inclined Riga surface. Shamshuddin and Narayana [22] discussed the effect of Joule heating and dissipation between two Riga plates with Cattaneo-Christov heat flux on the magnetohydrodynamic squeezing flow. Some recent attempts in this direction can be viewed via refs. [1, 19]. Non-Newtonian flows are more efficient due to their practical applications in physiological, technological processes and most industries. The properties of all non-Newtonian fluids are diverse, and the behaviors of all types of such fluids are depicted by a single relation. Williamson fluids elucidate such behaviors with more advantages than other fluids. Hamed et al. [12] investigated the two-dimensional incompressible Williamson nanofluid hydro magnetic flow over a stretching sheet in a porous media. A new mathematical model in a micropolar Williamson nanofluid for the flow of an electro-osmotic boundary layer are studied by Eldabe et al. [11]. Over an exponentially stretched surface, Jangid et al.[15] studied the heat transference to expand the hydro-magnetic Williamson fluid flow with nano-particles. Many results of the non-Newtonian are discussed in these articles [4, 13]. A solid-liquid mixture of tiny size nanoparticles and base liquid is known as nanofluid. The colloids of base liquid and nanoparticles have important physical characteristics which enhance their potential role in the applications of ceramics, drug delivery, paintings, coatings etc. Nanofluids are declared as super coolants because their heat absorption capacity is much higher than traditional liquids Eldabe et al. [7] studied the peristaltic unsteady flow of nanofluid non-Newtonian with heat transfer in vertical non-uniform duct. The flow follows the Herschel Bulkley model in a non-Darcy porous medium, considering thermal diffusion

and mixed convection. In a symmetric channel with compliant wall characteristics, the mixed convective peristaltic flow of Carreau-Yasuda nanofluid in the presence of slip conditions is discussed by Nisar et al [20]. Nowar [21] investigated the peristaltic flow of an incompressible conducting viscous electrically nanofluid through a porous medium in a vertical asymmetric channel with taking the Hall effects. Many results of the nanofluid are studied in these papers [3, 6, 8, 9, 14, 16]. The activation energy is a key concept in understanding the relationship between chemical reactions and the energy required for them to occur. The first mathematical connection between the rate of a chemical reaction and absolute temperature was given by Hood. Arrhenius extended Hood's idea to obtain the relation between the rate of chemical reaction and temperature, and the equation is usually called the Arrhenius equation. In the Arrhenius equation, the activation energy parameter refers to the minimum energy threshold that reactants must attain for a chemical reaction to occur and form new products. Muhammad et al. [17] investigated a mathematical analysis for three-dimensional Eyring-Powell thermal radiation nanofluid nonlinear with mass fluxes plus modified heat. The peristaltic waves of a non-Newtonian nanofluid along an asymmetric channel are investigated by taking activation energy and thermal radiation in consideration by Sara et al. [2]. This work attempts to fill the void of the movement of nano-non-Newtonian fluid obeying the Williamson model with heat and mass transfer through a porous medium over a stretching Riga sheet. The activation energy and modified Darcy law of the non-Newtonian fluid are considered. The non-linear partial differential equations that describe the motion were converted to ordinary differential equations using suitable transformations. The homotopy perturbation technique was used to solve this system subject to appropriate boundary conditions. The influences of relevant parameters were discussed graphically.

2. Mathematical formulation

The motion of non-Newtonian Williamson nanofluid with heat and mass transfer through porous medium with Williamson fluid over a stretching Riga plate is investigated. Choose Cartesian coordinates x and y , where x is in the direction of stretching sheet, and y is perpendicular to it as shown in figure (1). The activation energy, viscous dissipation and modified Darcy law for a porous medium are taken in our consideration. The constitutive equation of the Williamson model can be written as [12]

$$\underline{\tau} = \left(\mu_{\infty} + \frac{\mu_0 - \mu_{\infty}}{1 - \Gamma \nu^*} \right) \underline{A}, \quad (1)$$

where $\underline{A} = \nabla \underline{V} + \nabla^T \underline{V}$, $\nu^* = \sqrt{\frac{1}{2} \text{trace}(\underline{A}^2)}$, $\underline{\tau}$ is the stress tensor, μ_0 is the limiting viscosity, μ_{∞} is the viscosity at infinity, \underline{A} is the first Rivlin-Ericksen tensor, $\Gamma > 0$ is a time constant and $\underline{V}(u, v)$ is velocity.

In the case of $\mu_{\infty} = 0$, $\Gamma \nu^* < 1$, we get

$$\underline{\tau} = \mu_0(1 + \Gamma \nu^*) \underline{A}, \quad (2)$$

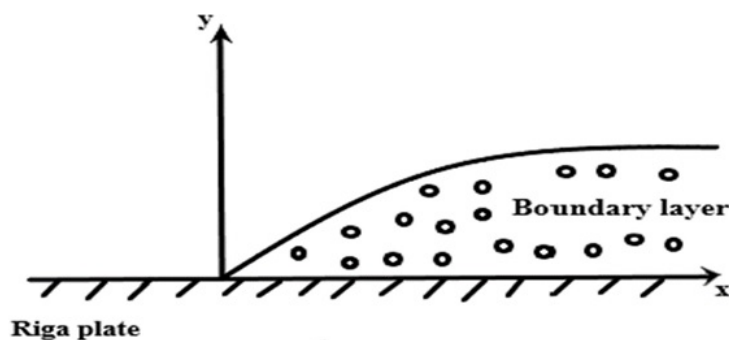


Figure 1: Sketch of the problem.

And have the following components

$$\begin{aligned}
 \tau_{xx} &= \mu_0 \left\{ 1 + \Gamma \sqrt{4 \left(\frac{\partial u}{\partial x} \right)^2 + \left(\frac{\partial u}{\partial y} + \frac{\partial v}{\partial x} \right)^2} \right\} 2 \frac{\partial u}{\partial x} \\
 \tau_{yy} &= \mu_0 \left\{ 1 + \Gamma \sqrt{4 \left(\frac{\partial u}{\partial x} \right)^2 + \left(\frac{\partial u}{\partial y} + \frac{\partial v}{\partial x} \right)^2} \right\} 2 \frac{\partial v}{\partial x} \\
 \tau_{xy} &= \mu_0 \left\{ 1 + \Gamma \sqrt{4 \left(\frac{\partial u}{\partial x} \right)^2 + \left(\frac{\partial u}{\partial y} + \frac{\partial v}{\partial x} \right)^2} \right\} \left\{ \frac{\partial u}{\partial y} + \frac{\partial v}{\partial x} \right\}
 \end{aligned} \tag{3}$$

Since, the magnetic force is generated by the Riga plate, the Lorentz force $\underline{f} = \underline{J} \wedge \underline{B}$ is defined as magnetic force. According to the Grinberg hypothesis this magnetic force is defined as

$$\underline{f} = \frac{\pi}{8} j_0 M_0 e^{-\frac{\pi}{l} y} \underline{i}, \tag{4}$$

where j_0 is the current density, M_0 is the constant magnetic field and l is the width of the plate. The boundary layer equations for the velocity, temperature and concentration can be written as follows:

$$\frac{\partial u}{\partial x} + \frac{\partial v}{\partial y} = 0 \tag{5}$$

$$u \frac{\partial u}{\partial x} + v \frac{\partial u}{\partial y} = \frac{\mu_0}{\rho_f} \frac{\partial}{\partial y} \left\{ 1 + \Gamma \frac{\partial u}{\partial y} \right\} \frac{\partial u}{\partial y} + \frac{\pi j_0 M_0}{8 \rho_f} e^{-\frac{\pi}{l} y} - \frac{\mu_0}{k_0 \rho_f} \left\{ 1 + \Gamma \frac{\partial u}{\partial y} \right\} u \tag{6}$$

$$u \frac{\partial T}{\partial x} + v \frac{\partial T}{\partial y} = \frac{k_c}{(\rho c)_f} \frac{\partial^2 T}{\partial y^2} + \tau_0 \left\{ D_B \frac{\partial T}{\partial y} \frac{\partial C}{\partial y} + \frac{D_T}{T_\infty} \left(\frac{\partial T}{\partial y} \right)^2 \right\} + \tag{7}$$

$$\frac{\mu_0}{(\rho c)_f} \left\{ 1 + \Gamma \frac{\partial u}{\partial y} \right\} \left(\frac{\partial u}{\partial y} \right)^2 - \frac{Q_0}{(\rho c)_f} (T - T_\infty) \\
 u \frac{\partial C}{\partial x} + v \frac{\partial C}{\partial y} = D_B \frac{\partial^2 C}{\partial y^2} + \frac{D_T}{T_\infty} \frac{\partial^2 T}{\partial y^2} - \lambda_0 \left(\frac{T}{T_\infty} \right)^m (C - C_\infty) e^{-\frac{E_a}{k_a T}} \tag{8}$$

where the last term in right hand side of equation (6) is due to the modified darcy law, where ρ_f is the fluid density, T is the fluid temperature, C is the fluid concentration, k_c is the thermal conductivity, D_B is the Brownian diffusion coefficient, D_T is the thermophoretic diffusion coefficient, $(\rho c)_p$ is the heat capacitance of the nanofluid, $\tau_0 = \frac{(\rho c)_p}{(\rho c)_f}$, $(\rho c)_f$ is the heat capacitance of the fluid, Q_0 is the constant heat absorption, λ_0 is chemical reaction coefficient, E_a is the activation energy, k_a is the Boltzmann constant and m is the fitted rate constant.

The appropriate boundary conditions are

$$\begin{aligned} u = ax, \quad v = 0, \quad T = T_w, \quad C = C_w, \quad y = 0 \\ u \rightarrow 0, \quad T \rightarrow T_\infty, \quad C \rightarrow C_\infty, \quad y \rightarrow \infty \end{aligned} \quad (9)$$

Consider the following similarity solutions to transform the system of our equations from non-linear partial differential equations to non-linear ordinary differential equations,

$$\begin{aligned} u = ax \frac{\partial f(\eta)}{\partial \eta}, \quad v = -\sqrt{av} f(\eta), \quad \eta = \sqrt{\frac{a}{\nu}} y \\ T = T_\infty + \theta(T_w - T_\infty), \quad C = C_\infty + \varphi(C_w - C_\infty) \end{aligned} \quad (10)$$

Where T_w is temperature at the Riga plate, C_w is the concentration at the Riga plate and T_∞ and C_∞ are the temperature and concentration at infinity respectively.

Then equations (6-8) become

$$f''' + 2We f'' f''' + f f'' - f'^2 - \frac{1}{k} f' - \frac{We}{k} f' f'' + M \exp(-s\eta) = 0 \quad (11)$$

$$\theta'' + Pr f \theta' + Nb Pr \theta' \varphi' + Nt Pr \theta'^2 + Pr N (f''^2 + We f''^3) - QPr\theta = 0 \quad (12)$$

$$\varphi'' + Sc f \varphi' + \frac{Nt}{Nb} \theta'' - Sc \lambda e^{-E} (E + m) (w - 1) \theta \varphi = 0 \quad (13)$$

With conditions

$$\begin{aligned} f = 0, \quad f' = 1, \quad \theta = 1, \quad \varphi = 1, \quad \eta = 0 \\ f' = 0, \quad \theta = 0, \quad \varphi = 0, \quad \eta \rightarrow \infty \end{aligned} \quad (14)$$

Where $We = \Gamma \frac{a^{\frac{3}{2}} x}{\sqrt{\nu}}$ is the Williamson parameter, $k = \frac{k_0 a}{\nu}$ is the permeability parameter, $M = \frac{\pi j_0 M_0}{8 \rho_f a^2 x}$ is the modified Hermann number, $s = \sqrt{\frac{\pi^2 \nu}{l^2 a}}$ is the dimensionless parameter, $Pr = \frac{\mu_0 c_f}{k_c}$ is the Prandtl number, $Nb = \frac{\tau_0 D_B (C_w - C_\infty)}{\nu}$ is the Brownian motion, $Nt = \frac{\tau_0 D_T (T_w - T_\infty)}{\nu T_\infty}$ is the thermophoresis variable, $Ec = \frac{a^2 x^2}{c_f (T_w - T_\infty)}$ is the dimensionless parameter, $Sc = \frac{\nu}{D_B}$ is the Schmidt number, $\lambda = \frac{\lambda_0}{a}$ is the chemical reaction parameter, $E = \frac{E_a}{k_a T_\infty}$ is the activation energy parameter and $w = \frac{T_w}{T_\infty}$ is the dimensionless parameter, $Q = \frac{Q_0}{(\rho c)_f a}$ is the heat absorption parameter.

3. Method of solutions

We shall use the homotopy perturbation method to obtain the semi-analytical solutions of equations (11-13) with boundary conditions (14).

The initial solutions can be written as

$$f_0(\eta) = 1 - e^{-\eta}, \quad \theta_0(\eta) = e^{-\eta} \quad \text{and} \quad \varphi_0(\eta) = e^{-\eta}. \quad (15)$$

Take the linear operator as $(D^3 - \frac{1}{k}D)$ to obtain the first and second order solutions of the velocity, $(D^2 - Q Pr)$ for temperature and $(D^2 - s_{47})$ for concentration. Now by using homotopy technique the velocity, temperature and concentration can be written as follows

$$\begin{aligned} f'(\eta) = & -s_{31}e^{-\eta} - s_{35}e^{-2\eta} + s_{36}e^{-3\eta} - s_{37}e^{-s\eta} - s_{38}e^{-\eta} \sqrt{1/k} \\ & + s_{39}e^{-\eta(1+s)} + s_{40}e^{-\eta(1+\sqrt{1/k})} + s_{41}\eta e^{-\eta\sqrt{1/k}}, \end{aligned} \quad (16)$$

$$\begin{aligned} \theta(\eta) = & s_{82}e^{-\eta} + s_{83}e^{-\eta\sqrt{Q Pr}} + s_{84}e^{-2\eta} + s_{840}e^{-3\eta} - s_{700}e^{-4\eta} \\ & - s_{72}\eta e^{-\eta\sqrt{Q Pr}} + s_{74}e^{-\eta(1+s)} - s_{75}e^{-\eta(1+\sqrt{Q Pr})} \\ & + s_{76}e^{-\eta(1+\sqrt{1/k})} + s_{77}e^{-\eta(1+\sqrt{s_{47}})} - s_{770}e^{-\eta(2+\sqrt{Q Pr})} \\ & - s_{771}e^{-\eta(2+s)}, \end{aligned} \quad (17)$$

$$\begin{aligned} \varphi(\eta) = & s_{111}e^{-\eta} + s_{112}e^{-2\eta} + s_{100}e^{-3\eta} + s_{1000}e^{-4\eta} - s_{113}e^{-\eta\sqrt{s_{47}}} \\ & + s_{101}\eta e^{-\eta\sqrt{s_{47}}} + s_{102}e^{-\eta(1+\sqrt{1/k})} + s_{103}e^{-\eta(1+s)} \\ & - s_{104}e^{-\eta\sqrt{Q Pr}} + s_{105}e^{-\eta(1+\sqrt{s_{47}})} + s_{106}e^{-\eta(1+\sqrt{Q Pr})}, \end{aligned} \quad (18)$$

3.1. Skin friction coefficient

The most important and interesting non-dimensional quantity that is the skin friction coefficient which is defined, evaluated and computed as

$$\tau_w = f'' + We f''^2 \quad (19)$$

For Williamson fluid, and at the wall $\eta = 0$, the skin friction becomes

$$\tau_w = s_{138} \quad (20)$$

Which is constant and functions of the physical parameters of the fluid.

3.2. Nusselt number

The Nusselt number in non-dimensional form can be written as

$$Nu = -\theta' \Big|_{\eta=0} \quad (21)$$

at the wall $\eta = 0$, the Nusselt number becomes

$$Nu = s_{143} \quad (22)$$

Which is constant and functions of the physical parameters of the fluid.

3.3. Sherwood number

The Sherwood number in dimensionless can be written as

$$Sh = -\varphi' \Big|_{\eta=0} \quad (23)$$

at the wall $\eta = 0$, the Sherwood number becomes

$$Sh = s_{148} \quad (24)$$

Which is constant and functions of the physical parameters of the fluid.

Here, s_0 - s_{148} are defined in the appendix.

4. Results and discussion

The aim of this section is to study the influences of activation energy with modified Darcy law for Williamson non-Newtonian fluid on the flow inside the boundary layer of a Riga plate through a porous medium. Heat and mass transfer are taken into account with heat absorption and chemical reaction. The system of equations is converted to nonlinear ordinary differential equations with boundary conditions using an appropriate transformation. The system is solved using the homotopy perturbation technique, and the velocity, temperature, and concentration distribution along with skin friction, Nusselt, and Sherwood numbers are obtained as a function of the physical parameters of the problem. Numerical calculations are used to investigate the influences of the physical parameters of the obtained solution. Additionally, the results are explained graphically through figures (2-21).

Figures (2-5) are plotted to illustrate the effects of M , k , s and We on the velocity $f'(\eta)$ for various values of the parameters of interest. It is shown from the figures that the velocity improves prominently with increasing the parameters M , k and We , while the velocity decreases with increasing s . The physical interpretation of these observations is due to the fluid moves in the boundary layer of the magnetic plate in the presence of a positive Lorentz force, which attracts the fluid to the plate and works to increase its speed directly with M . On the other hand, in the porous medium, there exist voids between the molecules of the fluid which allows the fluid velocity to increase with increasing k .

It can also be noted that since the term of magnetism that increases the speed, as we mentioned above, is multiplied by an exponential term with a negative strength s , it is mathematically clear that the speed of the fluid will decrease with an increase of s .

It is also clear that increasing the viscosity of the fluid, which occurs in the case of non-Newtonian fluids for the Williamson model, works to increase the velocity of the fluid in the boundary layer of the stretching sheet. Therefore, the velocity will increase with the increase of We .

Variation of temperature is illustrated in Figures (6-12). Figure (6) shows the magnetic field effect on temperature; an increase in magnetic field leads to a decrease in temperature. Also, as the permeability k of the medium increases and the gaps between its molecules increase, the temperature decreases, as shown in Figure (7). Figure (8) clarifies that the temperature slightly increases with increasing Brownian parameters Nb , due to the additional nanoparticles which enhance temperature. Variations of temperature components with s are shown in Figure (9). Temperature components increase with an increase in the constant s . Figure (11) illustrates that the temperature of the fluid rises as the value of Ec increases. This occurs because heat is generated within the fluid due to frictional heating as Ec increases. The effect of the Prandtl number on the temperature profile is shown in Figure (12). As the Prandtl number increases, the rate of thermal diffusion reduces, resulting in a constantly decreasing temperature profile. Physically, it follows that fluids with a high Prandtl number have high viscosity and low thermal conductivity, causing the fluid to thicken and decrease its velocity.

Figures (10) and (17) show that as the Williamson parameter increases, the temperature and concentration profiles, as well as the thickness of the boundary layer, also increase. This is due to reduced heat and mass transfer, as well as nanoparticle saturation within the boundary caused by drag against the non-Newtonian fluid stream. The presence of nanoparticles makes it ideal for use as a lubricant cooling agent, as they remain in the base fluid longer and enhance the flow characteristics of nanofluids.

The concentration profile rises for large values of activation energy E , as shown in Figure (13). An improvement in the concentration field results from the Arrhenius function deteriorating by snowballing the activation energy value, which promotes the generative chemical process. The effects of thermophoresis Nt on the concentration profile are depicted in Figure (14). This figure shows that as the thermophoresis parameter increases, the concentration profile rapidly increases at all places in the flow domain. Figure (15) shows how the chemical reaction parameter affects the concentration profiles. This figure shows that increasing values of λ have a significant effect on the concentration distribution in the boundary layer. It is apparent that the increasing values of λ lower the concentration in the boundary layer. Physically, large values of λ decrease the solute boundary layer thickness and promote mass transfer. Sc relates the relative thickness of the mass transfer layer to the hydrodynamic boundary layer. As a result, as Sc increases, mass diffusivity reduces, leading to a lower concentration, as shown in Figure (16). As the permeability parameter is raised, the concentration profile decreases. When the porous medium's permeability increases, it becomes more porous, which reduces the Darcian body force's magnitude and increases the rate at which mass transfers into the porous medium,

as shown in Figure (18). Figure (19) shows that an increase in Eckert number leads to a higher concentration. As the concentration increases, more radiation should be absorbed, resulting in an increase in absorbance; thus, concentration and absorption are directly proportional, as shown in Figure (20). Figure (21) demonstrates that Brownian motion reduces both concentration and thickness of the solute boundary layer. It is owing to the fact that increases in Brownian motion enhance the random movement that spreads the nanoparticles and hence decreases concentration.

Finally, the effects of the parameters of the problem on each of the skin friction τ_w , Nusselt number Nu, and Sherwood number Sh are discussed and illustrated in tables (1-3). Skin friction coefficients τ_w are calculated using the formula in Eq. 20. In Table (1a), the Williamson parameter We variety, while other parameters are fixed. The current study shows that skin friction increases with larger values of the Williamson parameter. This is because increasing the Williamson parameter thickens and makes the fluid more viscous. The magnetic field parameter M variety, while other parameters are fixed as shown in Table (1b). As M increases, the skin friction coefficient τ_w also increases. This is because a working magnetic field tends to enhance flow motion and, consequently, surface friction force in nanofluid flow. It has been observed that as a result of changing the parameters, this leads to change in the values of skin friction τ_w , which indicates the importance of the presence of external influences in the case of flow of non-Newtonian nanofluid inside the boundary layer of Riga magnetized surface. This has important scientific applications in various fields, such as paints, reactors and some medical devices. The Nusselt number increases as the magnetic field parameter increases, as shown in table (2). The table (3) explains how different values of Schmidt number influence the Sherwood number. The Sherwood number increases with an increase in the Schmidt number. The Schmidt number has a greater impact on the Sherwood number compared with the Nusselt number. For your information, other influences on all parameters were.

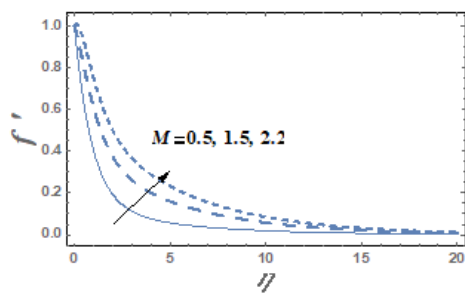


Figure 2: The variation of the velocity $f'(\eta)$ for various values of M .

$We = 0.5, s = 0.2, Nb = 0.4,$
 $Nt = 0.3, Ec = 5, Pr = 0.5,$
 $Q = 0.3, \lambda = 0.7, E = 0.7, Sc = 0.1,$
 $m = 0.5, w = 1, k = 0.3$

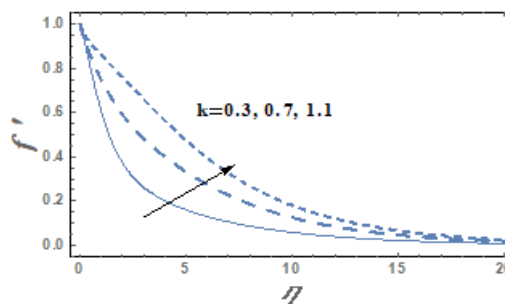


Figure 3: The variation of the velocity $f'(\eta)$ for various values of k .

$We = 0.5, s = 0.2, Nb = 0.4,$
 $Nt = 0.3, Ec = 5, Pr = 0.5,$
 $Q = 0.3, \lambda = 0.7, E = 0.7, Sc = 0.1,$
 $m = 0.5, w = 1$

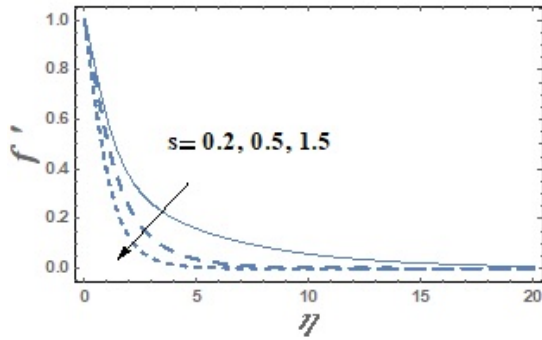


Figure 4: The variation of the velocity $f'(\eta)$ for various values of s .
 $We = 0.5, M = 1.5, Nb = 0.4,$
 $Nt = 0.3, Ec = 5, Pr = 0.5,$
 $Q = 0.3, \lambda = 0.7, E = 0.7, Sc = 0.1,$
 $m = 0.5, w = 1, k = 0.3$

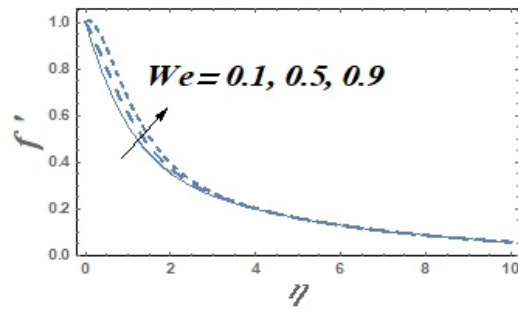


Figure 5: The variation of the velocity $f'(\eta)$ for various values of We .
 $M = 1.5, s = 0.2, Nb = 0.4,$
 $Nt = 0.3, Ec = 5, Pr = 0.5,$
 $Q = 0.3, \lambda = 0.7, E = 0.7, Sc = 0.1,$
 $m = 0.5, w = 1, k = 0.3$

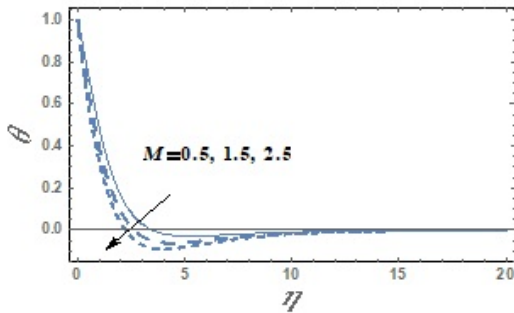


Figure 6: The variation of the temperature $\theta(\eta)$ for various values of M .
 $We = 0.5, s = 0.2, Nb = 0.4,$
 $Nt = 0.3, Ec = 5, Pr = 0.5,$
 $Q = 0.3, \lambda = 0.7, E = 0.7, Sc = 0.1,$
 $m = 0.5, w = 1, k = 0.3$

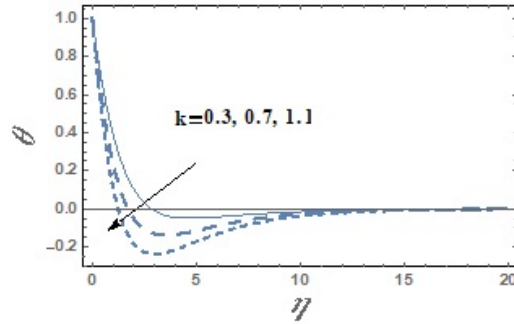


Figure 7: The variation of the temperature $\theta(\eta)$ for various values of k .
 $We = 0.5, M = 1.5, s = 0.2, Nb = 0.4,$
 $Nt = 0.3, Ec = 5, Pr = 0.5,$
 $Q = 0.3, \lambda = 0.7, E = 0.7, Sc = 0.1,$
 $m = 0.5, w = 1$

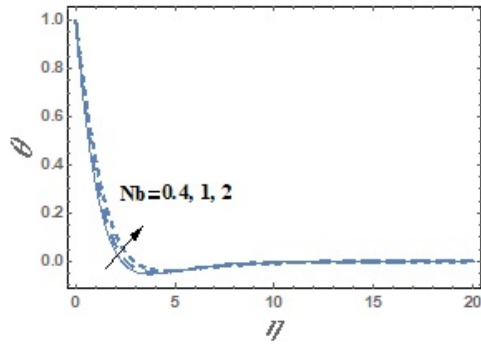


Figure 8: The variation of the temperature $\theta(\eta)$ for various values of Nb .
 $We = 0.5, M = 1.5, s = 0.2,$
 $Nt = 0.3, Ec = 5, Pr = 0.5,$
 $Q = 0.3, \lambda = 0.7, E = 0.7, Sc = 0.1,$
 $m = 0.5, w = 1, k = 0.3$

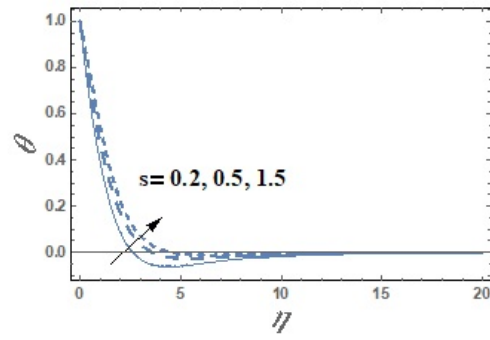


Figure 9: The variation of the temperature $\theta(\eta)$ for various values of s .
 $We = 0.5, M = 1.5, Nb = 0.4,$
 $Nt = 0.3, Ec = 5, Pr = 0.5,$
 $Q = 0.3, \lambda = 0.7, E = 0.7, Sc = 0.1,$
 $m = 0.5, w = 1, k = 0.3$

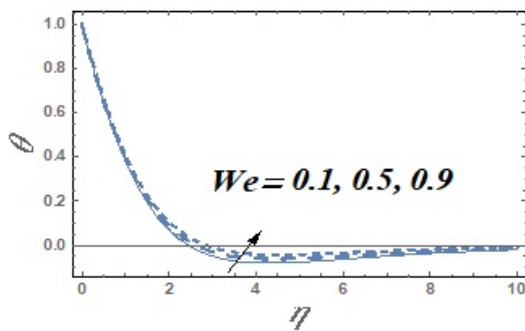


Figure 10: The variation of the temperature $\theta(\eta)$ for various values of We .
 $M = 1.5, s = 0.2, Nb = 0.4,$
 $Nt = 0.3, Ec = 5, Pr = 0.5,$
 $Q = 0.3, \lambda = 0.7, E = 0.7, Sc = 0.1,$
 $m = 0.5, w = 1, k = 0.3$

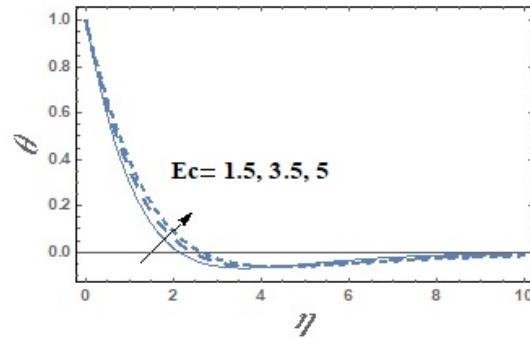


Figure 11: The variation of the velocity $\theta(\eta)$ for various values of Ec .
 $We = 0.5, M = 1.5, s = 0.2, Nb =$
 $0.4, Nt = 0.3, Pr = 0.5,$
 $Q = 0.3, \lambda = 0.7, E = 0.7, Sc = 0.1,$
 $m = 0.5, w = 1, k = 0.3$

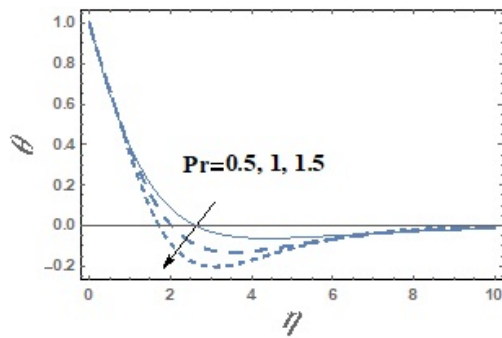


Figure 12: The variation of the velocity $\theta(\eta)$ for various values of Pr .

$We = 0.5, M = 1.5, s = 0.2, Nb = 0.4,$
 $Nt = 0.3, Ec = 5,$
 $Q = 0.3, \lambda = 0.7, E = 0.7, Sc = 0.1,$
 $m = 0.5, w = 1, k = 0.3$

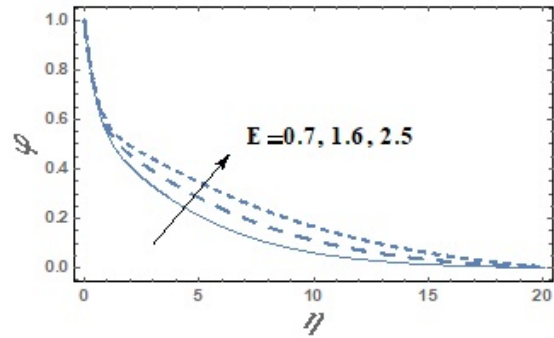


Figure 13: The variation of the velocity $\phi(\eta)$ for various values of E .

$We = 0.5, M = 1.5, s = 0.2, Nb = 0.4,$
 $Nt = 0.3, Ec = 5, Pr = 0.5,$
 $Q = 0.3, \lambda = 0.7, Sc = 0.1,$
 $m = 0.5, w = 1, k = 0.3$

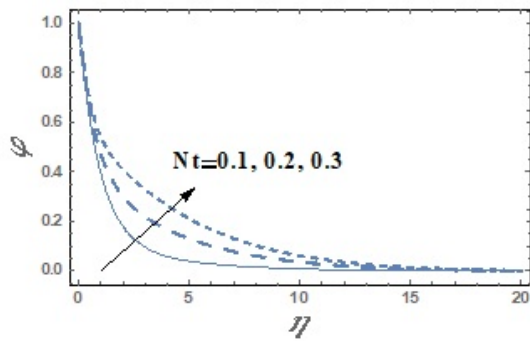


Figure 14: The variation of the velocity $\phi(\eta)$ for various values of Nt .

$We = 0.5, M = 1.5, s = 0.2, Nb = 0.4,$
 $Ec = 5, Pr = 0.5,$
 $Q = 0.3, \lambda = 0.7, E = 0.7, Sc = 0.1,$
 $m = 0.5, w = 1, k = 0.3$

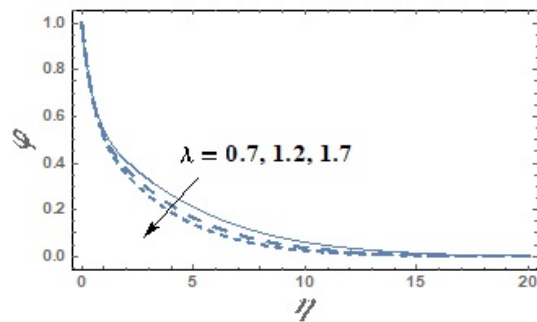


Figure 15: The variation of the concentration $\phi(\eta)$ for various values of λ

$We = 0.5, M = 1.5, s = 0.2, Nb = 0.4,$
 $Nt = 0.3, Ec = 5, Pr = 0.5,$
 $Q = 0.3, E = 0.7, Sc = 0.1,$
 $m = 0.5, w = 1, k = 0.3$

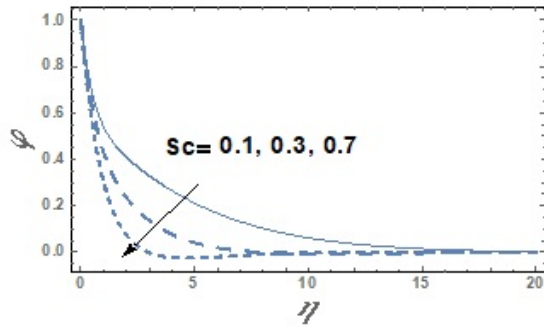


Figure 16: The variation of the velocity $\phi(\eta)$ for various values of Sc .

$We = 0.5, M = 1.5, s = 0.2, Nb = 0.4,$
 $Nt = 0.3, Ec = 5, Pr = 0.5,$
 $Q = 0.3, \lambda = 0.7, E = 0.7,$
 $m = 0.5, w = 1, k = 0.3$

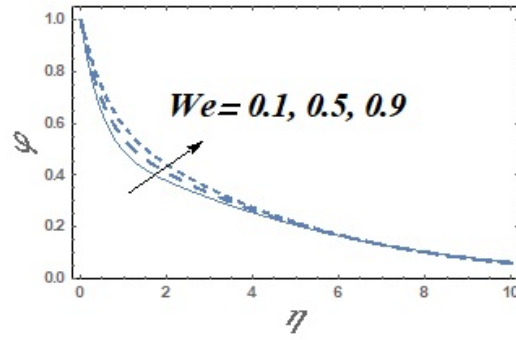


Figure 17: The variation of the velocity $\phi(\eta)$ for various values of We .

$M = 1.5, s = 0.2, Nb = 0.4,$
 $Nt = 0.3, Ec = 5, Pr = 0.5,$
 $Q = 0.3, \lambda = 0.7, E = 0.7, Sc = 0.1,$
 $m = 0.5, w = 1, k = 0.3$

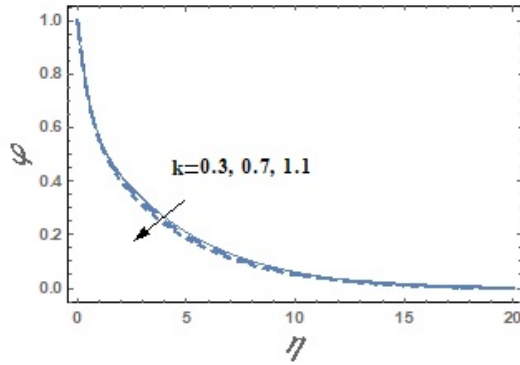


Figure 18: The variation of the velocity $\phi(\eta)$ for various values of k .

$We = 0.5, M = 1.5, s = 0.2, Nb = 0.4,$
 $Nt = 0.3, Ec = 5, Pr = 0.5,$
 $Q = 0.3, \lambda = 0.7, E = 0.7, Sc = 0.1,$
 $m = 0.5, w = 1$

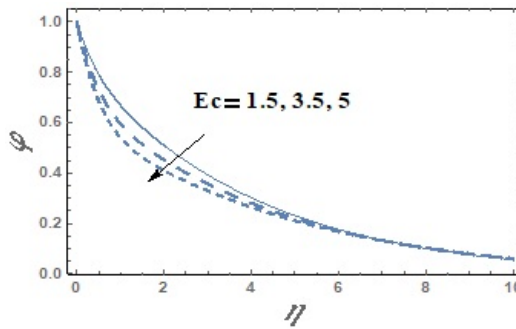


Figure 19: The variation of the velocity $\phi(\eta)$ for various values of Ec .

$We = 0.5, M = 1.5, s = 0.2, Nb = 0.4,$
 $Nt = 0.3, Pr = 0.5,$
 $Q = 0.3, \lambda = 0.7, E = 0.7, Sc = 0.1,$
 $m = 0.5, w = 1, k = 0.3$

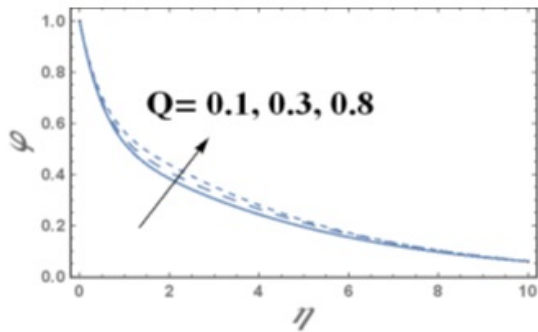


Figure 20: The variation of the velocity $\phi(\eta)$ for various values of Q .

$We = 0.5, M = 1.5, s = 0.2, Nb = 0.4, Nt = 0.3, Ec = 5, Pr = 0.5, \lambda = 0.7, E = 0.7, Sc = 0.1, m = 0.5, w = 1, k = 0.3$

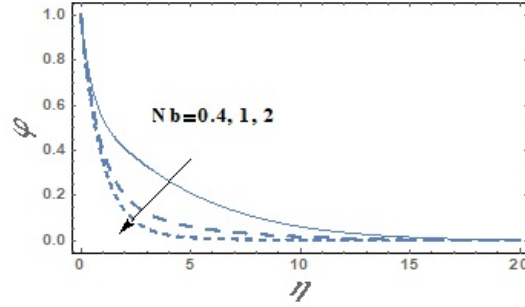


Figure 21: The variation of the velocity $\phi(\eta)$ for various values of Nb .

$We = 0.5, M = 1.5, s = 0.2, Nt = 0.3, Ec = 5, Pr = 0.5, Q = 0.3, \lambda = 0.7, E = 0.7, Sc = 0.1, m = 0.5, w = 1, k = 0.3$

We	k	M	Pr	sc	s	Ec	Nb	Nt	Q	λ	E	τ_w
0.1	0.3	1.5	0.5	0.1	0.2	5	0.4	0.3	0.3	0.7	0.7	-0.566953
0.3												-0.395052
0.5												-0.238782
0.9												0.223161

Table (1a). The computation results for local skin friction coefficient for variation of We .

We	k	M	Pr	sc	s	Ec	Nb	Nt	Q	λ	E	τ_w
0.5	0.3	0.5	0.5	0.1	0.2	5	0.4	0.3	0.3	0.7	0.7	-0.496554
		1.0										-0.418833
		1.5										-0.238782
		2.2										0.185204

Table (1b). The computation results for local skin friction coefficient for variation of M .

We	k	M	Pr	sc	s	Ec	Nb	Nt	Q	λ	E	Nu
0.5	0.3	0.5	0.5	0.1	0.2	5	0.4	0.3	0.3	0.7	0.7	0.522544
		1.0										0.672974
		1.5										0.823403
		2.2										1.034

Table (2). The computation results for local Nusselt number for variation of M .

We	k	M	Pr	sc	s	Ec	Nb	Nt	Q	λ	E	Sh
0.5	0.3	1.5	0.5	0.08	0.2	5	0.4	0.3	0.3	0.7	0.7	0.894771
				0.1								0.912382
				0.3								1.03737
				0.7								1.19726

Table (3). The computation results for local Sherwood number for variation of sc.

5. Conclusions

This study provides a comprehensive analysis of the complex interaction governing the Williamson non-Newtonian nanofluid flow over a Riga plate while incorporating the effects of activation energy, modified Darcy law, and thermal absorption. Heat and mass transfer have been included. With the necessary similarity variables, the set of nonlinear partial differential equations describing the velocity, temperature, and concentration are transformed into ordinary differential equations. Semi-analytical solutions using the homotopy perturbation method are obtained. The study indicates that velocity increases with increasing Williamson parameter, permeability parameter, and modified Hermann number, while it decreases with an increase in s. Increasing both the Brownian parameter and Eckert number affects the fluid’s temperature, causing it to increase. Also, increasing the permeability parameter, Prandtl number, and modified Hermann number decreases the temperature. Furthermore, nanoparticles concentration increases as the activation energy parameter, Williamson parameter and thermophoresis parameter increase. It was also concluded that the enhancement in both the chemical reaction, Schmidt number and Brownian parameter leads to a decrease in nanoparticle concentration. The study of fluid flow in the boundary layer adjacent to different surface, which is an important topic in fluid mechanics, is of great importance for many applications in various scientific fields, whether industry, such as the manufacture of aircraft, space vehicles and reactors. Also, in the painting works for different surfaces, and the manufacture of medical devices, as well as medical treatments. For future work and since the study of fluids flow is of great importance, we will use different models of non-Newtonian fluids that link the stress-rate of strain relationship. Also, an external magnetic field can be applied to the fluid motion and the ohmic dissipation due to magnetic field will take into consideration. In addition, we will study the problem when the fluid flows through porous media obeys non-darcy law.

Acknowledgements

The Researchers would like to thank the Deanship of Graduate Studies and Scientific Research at Qassim University for financial support (QU-APC-2025).

References

- [1] N Abbas and W Shatanawi. Heat and mass transfer of micropolar-casson nanofluid over vertical variable stretching riga sheet. *Energies*, 15:4945, 2022.
- [2] SI Abdelsalam, A Magesh, P Tamizharasi, and AZ Zaher. Versatile response of a sutterby nanofluid under activation energy: hyperthermia therapy. *International Journal of Numerical Methods for Heat & Fluid Flow*, 34(2):408–428, 2024.
- [3] SI Abdelsalam, KS Mekheimer, and AZ Zaher. Alterations in blood stream by electroosmotic forces of hybrid nanofluid through diseased artery: aneurysmal/stenosed segment. *Chinese Journal of Physics*, 67:314–329, 2020.
- [4] KK Asogwa, BS Goud, NA Shah, and SJ Yook. Rheology of electromagnetohydrodynamic tangent hyperbolic nanofluid over a stretching riga surface featuring dufour effect and activation energy. *Scientific Reports*, 12:14602, 2022.
- [5] S Bilal, KK Asogwa, H Alotaibi, MY Malik, and I Khan. Analytical treatment of radiative casson fluid over an isothermal inclined riga surface with aspects of chemically reactive species. *Alexandria Engineering Journal*, 60:4243–4253, 2021.
- [6] NTM El-Dabe, MY Abou-zeid, MA Mohamed, and MM Abd-Elmoneim. Peristaltic mixed convection slip flow of a bingham nanofluid through a non-darcy porous medium in an inclined non-uniform duct with viscous dissipation and radiation. *Journal of Applied Nonlinear Dynamics*, 12(02):231–243, 2023.
- [7] NTM El-dabe, MY Abou-zeid, MA Mohamed, and M Maged. Peristaltic flow of herchel bulkley nanofluid through a non-darcy porous medium with heat transfer under slip condition. *International Journal of Applied Electromagnetics and Mechanics*, 66:649–668, 2021.
- [8] NTM El-dabe, MY Abou-zeid, and YM Younis. Magnetohydrodynamic peristaltic flow of jeffry nanofluid with heat transfer through a porous medium in a verticle tube. *Appl Math Inf Sci*, 11(4):1097–1103, 2017.
- [9] NTM El-Dabe, Y Mohamed MY Abou-zeid, MAA Mohamed, and MM Abd-Elmoneim. Peristaltic mixed convection slip flow of a bingham nanofluid through a non-darcy porous medium in an inclined non-uniform duct with viscous dissipation and radiation. *Journal of Applied Nonlinear Dynamics*, 12:231–243, 2023.
- [10] NTM Eldabe, M Gabr, E Mahmoud, A Zaher, and S Zaher. The effect of Joule heating and viscous dissipation on the boundary layer flow of a magnetohydrodynamics micropolar-nanofluid over a stretching vertical Riga plate. *Heat Transfer*, 50(3):4788–4805, 2021.
- [11] NTM Eldabe, SA Hussein, ME Gabr, and AZ Zaher. A novel mathematical model of mhd boundary layer flow of an activated micropolar nanofluid over a stretching surface under the effect of electro-osmosis forces. *Modern Physics Letters B*, 37:2350153, 2023.
- [12] MS Hamed, NTM Eldabe, KA Kamel, EA Abd-Aziz, and HM Shawky. Mhd flow with heat and mass transfer of williamson nanofluid over stretching sheet through porous medium. *Microsystem technologies*, 25:1155–1169, 2019.
- [13] T Hayat, B Ahmed, FM Abbasi, and A Alsaedidi. Numerical investigation for peristaltic flow of carreau–yasuda magneto-nanofluid with modified darcy and radiation.

- Journal of Thermal Analysis and Calorimetry*, 137:1359–1367, 2019.
- [14] T Hayat, A Aziz, T Muhammad, and A Alsaedi. Model and comparative study for flow of viscoelastic nanofluids with cattaneo-christov double diffusion. *PLoS One*, 12:e0168824, 2017.
- [15] S Jangid, R Mehta, A Bhatnagar, MF Alotaibi, and H Ahmad. Heat and mass transfer of hydromagnetic williamson nanofluid flow study over an exponentially stretched surface with suction/injection, buoyancy, radiation and chemical reaction impacts. *Case Studies in Thermal Engineering*, 59:104278, 2024.
- [16] MY Mohameda, NTM Eldabe, MY Abou-zeid, ME Oauf, and DR Mostapha. Peristaltic transport of carreau coupled stress nanofluid with cattaneo-christov heat flux model inside a symmetric channel. *J. Adv. Res. Fluid Mech. Therm. Sci*, 98:1–17, 2022.
- [17] T Muhammad, H Waqas, SA Khan, R Ellahi, and SM Sait. Significance of nonlinear thermal radiation in 3d eyring–powell nanofluid flow with arrhenius activation energy. *Journal of Thermal Analysis and Calorimetry*, 143:929–944, 2021.
- [18] M Naseer, M Malik, Y Muhammad, S Nadeem, and A Rehman. The boundary layer flow of hyperbolic tangent fluid over a vertical exponentially stretching cylinder. *Alexandria engineering journal*, 53:747–750, 2014.
- [19] S Nasrin, RN Mondal, and MM Alam. Unsteady couette flow past between two horizontal rigid plates with hall and ion slip effects. *Math. Stat.*, 9:552–565, 2021.
- [20] Z Nisar, T Hayat, A Alsaedi, and S Momani. Peristaltic flow of chemically reactive carreau-yasuda nanofluid with modified darcy’s expression. *Materials Today Communications*, 33:104532, 2022.
- [21] K Nowar. Peristaltic flow of a nanofluid under the effect of hall current and porous medium. *Mathematical Problems in Engineering*, 2014:389581, 2014.
- [22] MD Shamsuddin and PV Satya Narayana. Combined effect of viscous dissipation and joule heating on mhd flow past a rigid plate with cattaneo–christov heat flux. *Indian Journal of Physics*, 94:1385–1394, 2020.

Appendix

$$\begin{aligned}
s_0 &= (2 - 1/k) We, s_1 = \frac{s_0}{2(4 - 1/k)}, s_2 = \frac{M}{s(s^2 - 1/k)}, s_3 = \frac{k}{k - 1}, \\
s_4 &= s_1 + s_3 - s_2, s_5 = \sqrt{k}(s_3 + 2s_1 - s s_2), s_6 = s_4 - s_5, \\
s_7 &= 24s_1 We - s_1 - \frac{6s_1 We}{k}, s_8 = 4We s_3 + 4s_1 - \frac{2s_3 We}{k}, \\
s_9 &= s_3 + s_6, s_{10} = s_2 - 2We s_2 s^2 (s + 1), s_{11} = s s_2 (s - 2) + \frac{We s s_2}{k} (s + 1), \\
s_{12} &= s_{10} + s_{11}, s_{13} = \frac{-2 We s_5 (1 + \sqrt{1/k})}{k} + \frac{s_5 We (1 + k \sqrt{1/k})}{k^2}, \\
s_{14} &= \frac{s_5}{k^2} (k + k^2 2k^2 \sqrt{1/k}), s_{15} = s_{13} + s_{14}, s_{16} = \frac{s_5}{k}, \\
s_{17} &= s^2 s_2, s_{18} = \frac{s_7}{3(9 - \frac{1}{k})}, s_{19} = \frac{s_8}{2(4 - \frac{1}{k})}, s_{20} = s_9 / (1 - 1/k), \\
s_{21} &= \frac{s_{12}}{(1 + s) \left((1 + s)^2 - \frac{1}{k} \right)}, s_{22} = \frac{s_{15}}{(1 + \sqrt{1/k}) (1 + 2\sqrt{1/k})}, s_{23} = \frac{k s_{16}}{2}, \\
s_{24} &= \frac{s_{17}}{s(s^2 - \frac{1}{k})}, s_{25} = s_{18} + s_{19} + s_{20} + s_{21} + s_{22} - s_{24}, s_{26} = \sqrt{k}(3s_{18} + 2s_{19} + s_{20}), \\
s_{27} &= \sqrt{k} (s_{21} (1 + s) + s_{22} (1 + \sqrt{1/k}) - s_{23} - s s_{24}), s_{28} = s_{26} + s_{27}, s_{29} = s_{25} - s_{28}, \\
s_{30} &= 1 + s_6 + s_{29}, s_{31} = - (1 + s_3 + s_{20}), s_{32} = - (s_1 + s_{19}), \\
s_{33} &= s_2 + s_{24}, s_{34} = s_5 + s_{28}, s_{35} = 2s_{32}, s_{36} = 3 s_{18}, s_{37} = s s_{33}, \\
s_{38} &= s_{34} \sqrt{1/k} + s_{23}, s_{39} = (1 + s) s_{21}, s_{40} = (1 + \sqrt{1/k}) s_{22},
\end{aligned}$$

$$s_{41} = s_{23}\sqrt{1/k}, s_{42} = Pr(1 + Nt + Nb + Ec), s_{43} = Pr, \quad s_{430} = PrEcW,$$

$$s_{44} = \frac{s_{42}}{4 - QPr}, \quad s_{45} = \frac{s_{43}}{1 - QPr}, \quad s_{450} = \frac{s_{430}}{9 - QPr}, \quad s_{46} = s_{44} - s_{45} - s_{450},$$

$$s_{47} = sc \lambda e^{-E}, \quad s_{48} = s_{47}(E + m)(w - 1), \quad s_{49} = s_{48} - sc, \quad s_{50} = sc - \frac{Nt}{Nb},$$

$$s_{51} = \frac{s_{49}}{4 - s_{47}}, \quad s_{52} = \frac{s_{50}}{1 - s_{47}}, \quad s_{53} = s_{51} + s_{52},$$

$$s_{54} = Pr(s_6 + s_{45}), \quad s_{55} = Pr(2s_{44} + s_{45} + s_3 + Nb s_{52}),$$

$$s_{56} = Pr(-Nb s_{45} - 2Nt s_{45} - 2Ec s_3), \quad s_{57} = s_{56} - s_{55},$$

$$s_{58} = Pr(2s_{44} - s_1 - 2Nb s_{51}), \quad s_{59} = Pr(2Nbs_{44} + 4Nts_{44} - 8Ec s_1),$$

$$s_{590} = 3Pr(s_{450} + EcWe s_3), \quad s_{60} = s_{58} + s_{59} + s_{590},$$

$$s_{600} = 3Pr(s_{450} + Nb s_{450} + 2Nt s_{450} - 4EcWe s_1),$$

$$s_{62} = Pr s_{46} \sqrt{QPr}, \quad s_{64} = Pr(s_2 + 2Ec s^2 s_2),$$

$$s_{65} = Pr \sqrt{QPr}(s_{46} + Nb s_{46} + 2Nt s_{46}), \quad s_{66} = Pr s_5 \left(1 + \frac{2Ec}{k}\right),$$

$$s_{67} = Pr Nb s_{53} \sqrt{s_{47}}, \quad s_{670} = \frac{3We Ec s_5 Pr}{k}, \quad s_{671} = 3We Pr Ec s^2 s_2,$$

$$s_{68} = \frac{s_{54}}{1 - Q Pr}, \quad s_{69} = \frac{s_{57}}{4 - Q Pr}, \quad s_{70} = \frac{s_{60}}{9 - Q Pr},$$

$$s_{700} = \frac{s_{600}}{16 - Q Pr}, \quad s_{72} = \frac{s_{62}}{2 \sqrt{Q Pr}}, \quad s_{74} = \frac{s_{64}}{(1 + s)^2 - Q Pr},$$

$$s_{75} = \frac{s_{65}}{1 + 2 \sqrt{Q Pr}}, \quad s_{76} = \frac{s_{66}}{\left(1 + \sqrt{1/k}\right)^2 - Q Pr},$$

$$s_{77} = \frac{s_{67}}{\left(1 + \sqrt{s_{47}}\right)^2 - Q Pr}, \quad s_{770} = \frac{s_{670}}{\left(2 + \sqrt{1/k}\right)^2 - Q Pr}, \quad s_{771} = \frac{s_{671}}{(2 + s)^2 - Q Pr},$$

$$s_{78} = s_{68} + s_{69} + s_{70}, \quad s_{79} = s_{771} + s_{700} + s_{770} + s_{75},$$

$$s_{80} = s_{74} + s_{76} + s_{77}, \quad s_{81} = s_{78} - s_{79} + s_{80}, \quad s_{82} = 1 + s_{45} + s_{68},$$

$$s_{83} = s_{46} - s_{81}, \quad s_{84} = s_{69} - s_{44}, \quad s_{840} = s_{70} + s_{450},$$

$$s_{85} = sc (s_{52} + s_6) - \frac{Nt}{Nb} s_{45}, \quad s_{86} = sc (2s_{51} - s_{52} - s_3),$$

$$s_{87} = (4 Nt)/Nb s_{44} + s_{48} s_{52} + s_{48} s_{45}, \quad s_{88} = s_{86} + s_{87},$$

$$s_{89} = sc (s_1 + 2s_{51}) + 9 \frac{Nt}{Nb} s_{450}, \quad s_{90} = s_{48} (s_{51} - s_{44}),$$

$$s_{91} = s_{90} - s_{89}, \quad s_{910} = s_{48} s_{450}, \quad s_{92} = sc s_{53} \sqrt{s_{47}}, \quad s_{93} = sc s_5,$$

$$s_{94} = sc s_2, \quad s_{95} = \frac{Nt}{Nb} s_{46} Q Pr, \quad s_{96} = s_{53} (sc \sqrt{s_{47}} - s_{48}),$$

$$s_{97} = s_{48} s_{46}, \quad s_{98} = \frac{s_{85}}{1 - s_{47}}, \quad s_{99} = \frac{s_8}{4 - s_{47}}, \quad s_{100} = \frac{s_{91}}{9 - s_{47}},$$

$$s_{1000} = \frac{s_{910}}{16 - s_{47}}, \quad s_{101} = \frac{s_{91}}{2\sqrt{s_{47}}}, \quad s_{102} = \frac{s_{93}}{\left(1 + \sqrt{1/k}\right)^2 - s_{47}},$$

$$s_{103} = \frac{s_{94}}{(1 + s)^2 - s_{47}}, \quad s_{104} = \frac{s_{95}}{Q Pr - s_{47}}, \quad s_{105} = \frac{s_{96}}{1 + 2\sqrt{s_{47}}},$$

$$s_{106} = \frac{s_{97}}{\left(1 + \sqrt{Q Pr}\right)^2 - s_{47}}, \quad s_{107} = s_{98} + s_{99} + s_{100} + s_{1000},$$

$$s_{108} = s_{102} + s_{103}, \quad s_{109} = s_{105} + s_{106},$$

$$s_{110} = s_{107} + s_{108} + s_{109} - s_{104}, \quad s_{111} = 1 + s_{98} + s_{52},$$

$$s_{112} = s_{51} + s_{99}, \quad s_{113} = s_{110} + s_{53}, \quad s_{114} = 2 s_{35}, \quad s_{115} = 3 s_{36},$$

$$s_{116} = s s_{37}, \quad s_{117} = s_{38}\sqrt{1/k} + s_{41}, \quad s_{118} = s_{39}(1 + s),$$

$$s_{119} = s_{40}\left(1 + \sqrt{1/k}\right), \quad s_{120} = s_{41}\sqrt{1/k},$$

$$s_{121} = s_{31} + s_{114} - s_{115} + s_{116}, \quad s_{122} = s_{117} - s_{118} - s_{119},$$

$$s_{123} = s_{121} + s_{122}, \quad s_{124} = (s_{31})^2 + (s_{114})^2 + (s_{115})^2 + (s_{116})^2,$$

$$s_{125} = (s_{117})^2 + (s_{118})^2 + (s_{119})^2, \quad s_{126} = 2s_{31}(s_{114} - s_{115} + s_{116}),$$

$$s_{127} = 2s_{31}(s_{117} - s_{118} - s_{119}), \quad s_{128} = 2s_{114}(s_{116} - s_{115} + s_{117}),$$

$$s_{129} = 2s_{114}(s_{118} + s_{119}), \quad s_{130} = 2s_{115}(s_{116} + s_{117} - s_{118} - s_{119}),$$

$$s_{131} = 2s_{116} (s_{117} - s_{118} - s_{119}), \quad s_{132} = 2s_{117} (s_{118} + s_{119}),$$

$$s_{133} = 2s_{118} s_{119}, \quad s_{134} = s_{124} + s_{125} + s_{126} + s_{126},$$

$$s_{135} = s_{128} - s_{129} - s_{130}, \quad s_{136} = s_{131} - s_{132} + s_{133},$$

$$s_{137} = s_{134} + s_{135} + s_{136}, \quad s_{138} = s_{123} + We s_{137},$$

$$s_{139} = s_{82} + s_{83} \sqrt{Q Pr} + 2s_{84}, \quad s_{140} = 4s_{700} + s_{770} (2 + \sqrt{1/k}) - 3s_{840},$$

$$s_{141} = s_{75} (1 + \sqrt{Q Pr}) - s_{74} (1 + s) + s_{771} (2 + s),$$

$$s_{142} = s_{76} (1 + \sqrt{1/k}) + s_{77} (1 + \sqrt{s_{47}}) + s_{72},$$

$$s_{143} = s_{139} - s_{140} - s_{141} + s_{142}, \quad s_{144} = s_{111} + 2s_{112} + 3s_{100},$$

$$s_{145} = s_{102} (1 + \sqrt{1/k}) - s_{113} \sqrt{s_{47}},$$

$$s_{146} = s_{103} (1 + s) - s_{101} - s_{104} \sqrt{Q Pr},$$

$$s_{147} = 4s_{1000} + s_{106} (1 + \sqrt{Q Pr}) + s_{105} (1 + \sqrt{s_{47}}),$$

$$s_{148} = s_{144} + s_{145} + s_{146} + s_{147}.$$